HNPS Advances in Nuclear Physics

Vol 27 (2019)

HNPS2019

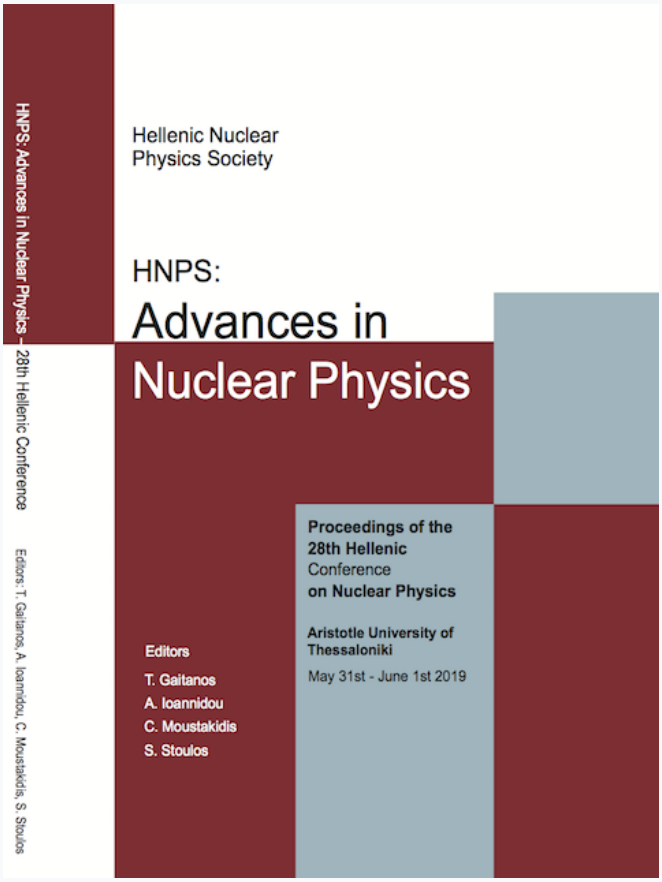

Microscopic description of induced fission dynamics with nuclear energy density functionals

Vaia Prassa, H Tao, J. Zhao, Z. P. Li, T. Nikšić, D. Vretenar

doi: 10.12681/hnps.3000

Microscopic description of induced fission dynamics with nuclear energy density functionals

V. Prassa[1], H. Tao[2], J. Zhao[3,4], Z. P. Li[2], T. Nikšić[4], and D. Vretenar[4]

[1] *Department of Computer Science, Faculty of Sciences, University of Thessaly, Greece*
[2] *School of Physical Science and Technology, Southwest University, China*
[3] *Microsystem & Terahertz Research Center, China Academy of Engineering Physics, China*
[4] *Physics Department, Faculty of Science, University of Zagreb, Croatia*

Abstract *Static and dynamic aspects of the fission process are analyzed in a self-consistent framework based on energy density functionals. Multidimensionally constrained mean-field calculations in the collective space determine the potential energy surface of the fissioning nucleus, the scission line, the single-nucleon wave functions, energies, and occupation probabilities. Induced fission dynamics is described using the time-dependent generator coordinate method in the Gaussian overlap approximation. The position of the scission line is analyzed as a function of the strength of the pairing interaction, as well as the effect of static pairing correlations on charge yields and total kinetic energy of fission fragments [1].*

Keywords *nuclear fission, density functionals, collective models*

Corresponding author: V. Prassa (vprassa@gmail.com) | *Published online:* May 1st, 2020

INTRODUCTION

Nuclear fission is the process revealing most clearly the complexity of low–energy nuclear dynamics. Thus, it provides an ideal test for the modeling of nuclear systems with quantum many–body theories. The theoretical description of the nuclear fission phenomenon remains one of the major challenges of quantum many–body dynamics. In order for fission to occur, nuclei have to overcome the fission barrier, which involves dissipative motion. The slow large–amplitude collective motion of the compound system that eventually leads to the formation of the final fragments can be described, in a first approximation, as an adiabatic process in which the intrinsic nucleonic degrees of freedom are decoupled from macroscopic collective degrees of freedom such as multipole moments (deformations) of the mass distribution and pairing fields [2,3].

The spontaneous or induced fission process in which a heavy nucleus splits into fragments is out of reach for ab initio methods and, therefore, modern microscopic approaches are based on the framework of nuclear energy density functionals (NEDFs). Nuclear density functional theory (DFT) and its time-dependent (TD) generalization have enabled a self consistent treatment of both static and dynamic aspects of fission [4–12]. Numerous studies of spontaneous fission, based on NEDFs, have analyzed the effects of the choice of collective coordinates (shape degrees of freedom), approximations used to calculate the collective inertia, and coupling between shape and pairing degrees of freedom on fission half–lives [13–19].

A microscopic approach capable of predicting both the low-energy collective excitation spectra in the deformed equilibrium minimum and the fission fragment distribution is the generator coordinate method (GCM). In the Gaussian overlap approximation (GOA) the GCM Hill–Wheeler equation reduces to a local Schrödinger–like equation in the space of collective coordinates. For a specific choice of collective coordinates, the essential inputs are the potential and inertia tensor that can be computed microscopically in a self–consistent mean-field deformation–constrained calculation. In particular, several recent studies have used the time-dependent generator coordinate

method (TDGCM) [20] to compute the induced fission fragment charge and mass distributions [21–25].

THEORETICAL FRAMEWORK

In the present study we consider the axial deformation parameters: quadrupole β_2 and octupole β_3. A time–dependent Schrödinger–like equation describes low–energy fission dynamics, and this equation can be derived using the time dependent generator coordinate method (TDGCM) in the Gaussian overlap approximation (GOA) [2,24]:

$$i\hbar\frac{\partial}{\partial t}g(\beta_2,\beta_3,t)=\left[-\frac{\hbar^2}{2}\sum_{kl}\frac{\partial}{\partial\beta_k}B_{kl}(\beta_2,\beta_3)\frac{\partial}{\partial\beta_l}+V(\beta_2,\beta_3)\right]\times g(\beta_2,\beta_3,t) \quad (1)$$

where $g(\beta_2,\beta_3,t)$ denotes the complex wave function of the collective variables (β_2,β_3) and time t. $V(\beta_2,\beta_3)$ and $B_{kl}(\beta_2,\beta_3)$ are the collective potential and mass tensor, respectively, and they completely determine the dynamics of the fission process in the TDGCM+GOA framework. These quantities will here be calculated in a self-consistent mean field approach based on relativistic energy density functionals. For the time-evolution we follow the method of Refs. [23,24] and make use of the software package FELIX [23] that solves the equations of the TDGCM in N dimensions under the Gaussian overlap approximation.

From the Schrödinger-like Eq. (1) a continuity equation for the probability density $|g(\beta_2,\beta_3,t)|^2$ is obtained,

$$\frac{\partial}{\partial t}|g(\beta_2,\beta_3,t)|^2=-\boldsymbol{\nabla}\boldsymbol{J}(\beta_2,\beta_3,t) \quad (2)$$

where $\boldsymbol{J}(\beta_2,\beta_3,t)$ is the probability current defined by the relation:

$$J_k(\beta_2,\beta_3,t)=\frac{\hbar}{2i}\sum_{l=2}^{3}B_{kl}(\beta_2,\beta_3)\left[g^*(\beta_2,\beta_3,t)\frac{\partial g(\beta_2,\beta_3,t)}{\partial\beta_l}-g(\beta_2,\beta_3,t)\frac{\partial g^*(\beta_2,\beta_3,t)}{\partial\beta_l}\right] \quad (3)$$

The collective space is divided into the inner region in which the nuclear density distribution is whole, and an external region that contains the two fission fragments. The set of scission configurations defines the hypersurface that separates the two regions. The flux of the probability current through this hypersurface provides a measure of the probability of observing a given pair of fragments at time t. For a surface element ξ on the scission hypersurface, the integrated flux *F(ξ, t)* is defined as [23]:

$$\boldsymbol{F(\xi,t)}=\int_{t=0}^{t}\boldsymbol{dt}\int_{(\boldsymbol{\beta_2},\boldsymbol{\beta_3})\in\xi}\boldsymbol{J(\beta_2,\beta_3,t)}\cdot\boldsymbol{dS} \quad (4)$$

For each scission point, (A_L,A_H) denote the masses of the lighter and heavier fragments, respectively. Therefore, the yield for the fission fragment with mass A can be defined by

$$Y(A)\propto\sum_{\xi\in A}\lim_{t\to+\infty}F(\xi,t) \quad (5)$$

where A is the set of all elements ξ belonging to the scission hypersurface such that one of the fragments has mass A.

RESULTS AND DISCUSSION

In this section we present the results of an illustrative study of induced fission of ^{226}Th, for which the charge distribution of fission fragments exhibits a coexistence of symmetric and asymmetric peaks [26]. In the first step a large–scale deformation–constrained self–consistent RMF+BCS calculation is performed to generate the potential energy surface and single-nucleon wave functions in the (β_2, β_3) plane. The range of collective variables is −0.83−6.01 for β_2 with a step $\Delta\beta$ = 0.04, and from 0.01–3.53 for β_3 with a step $\Delta\beta_3$ = 0.08. The energy density functional PC–PK1 [27] is used for the effective interaction in the particle–hole channel, and a δ–force pairing with strengths parameters:

V_n=360 MeV•fm^3 and V_p=378 MeV•fm^3 determined by the empirical pairing gap parameters of ^{226}Th, calculated using a five–point formula [28]. The self–consistent Dirac equation for the single–particle wave functions is solved by expanding the nucleon spinors in an axially deformed harmonic oscillator basis in cylindrical coordinates with 20 major shells. The computer code FELIX [23] is used for modeling the time evolution of the fissioning nucleus with a time step $\delta t=5\cdot10^{-4}$ zs. The parameters of the additional imaginary absorption potential that takes into account the escape of the collective wave packet in the domain outside the region of calculation [23] are: the absorption rate $r=20\cdot10^{22}$ s^{-1}, and the width of the absorption band w=1.5.

The present RMF+BCS results for the potential energy surface (PES), scission line, and total kinetic energy of ^{226}Th can be compared to those obtained in Ref. [29] using the Hartree-Fock-Bogoliubov framework based on the Gogny D1S effective interaction. Figure 1 displays the self-consistent RMF+BCS quadrupole and octupole constrained energy surfaces, the static fission path, and density distributions for selected deformations along the fission path of ^{226}Th. The lowest minimum is located at (β_2, β_3) ~ (0.20,0.17), but is rather soft against octupole deformation. A triple-humped fission barrier is predicted along the static fission path, and the calculated heights are 7.10, 8.58, and 7.32 MeV from the inner to the outer barrier, respectively. At elongations $\beta_2 > 1.5$ a symmetric valley extends up to the scission point at $\beta_2 \sim 5.4$. The symmetric and asymmetric fission valleys are separated by a ridge from (β_2, β_3) = (1.6,0.0) to (3.4,1.0). One notices that the overall topography of the PES is similar to that calculated with the Gogny D1S interaction [29].

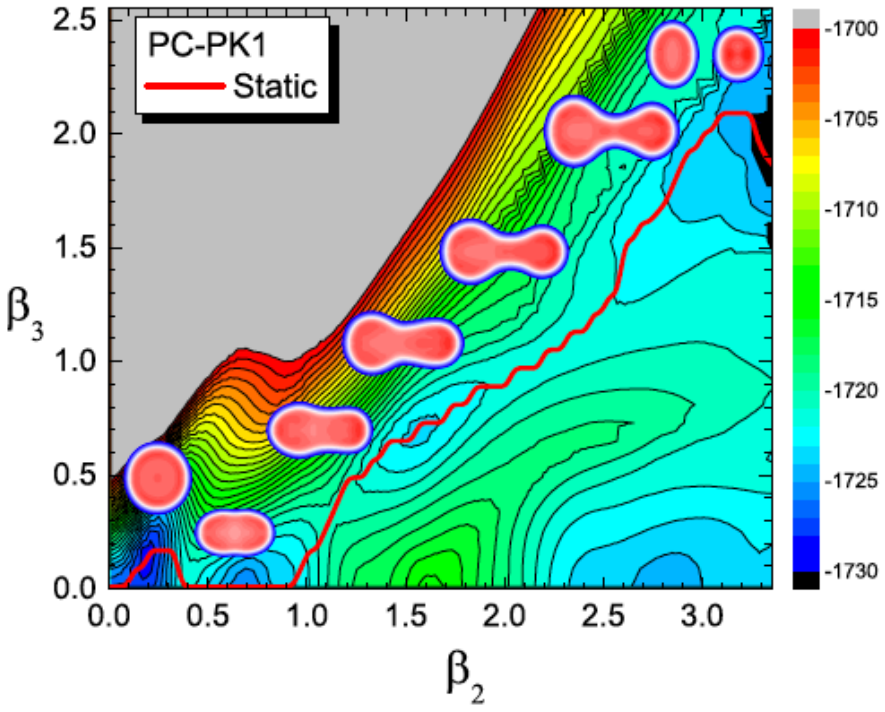

Figure 1. *Self–consistent RMF+BCS quadrupole and octupole constrained deformation energy surface (in MeV) of ^{226}Th in the β_2–β_3 plane.*

When describing fission in the β_2-β_3 collective space, scission is characterized by a discontinuity between the two domains of prescissioned and postscissioned configurations. Scission can be described using the Gaussian neck operator $Q_N = \exp[-(z - z_N)^2/a_N^2]$, where a_N = 1 fm and z_N is the position of the neck [30]. It is related to the number of particles in the neck, and here we follow the prescription of Ref. [24] to define the prescission domain by $\langle Q_N \rangle > 3$ and consider the frontier of this domain as the scission line.

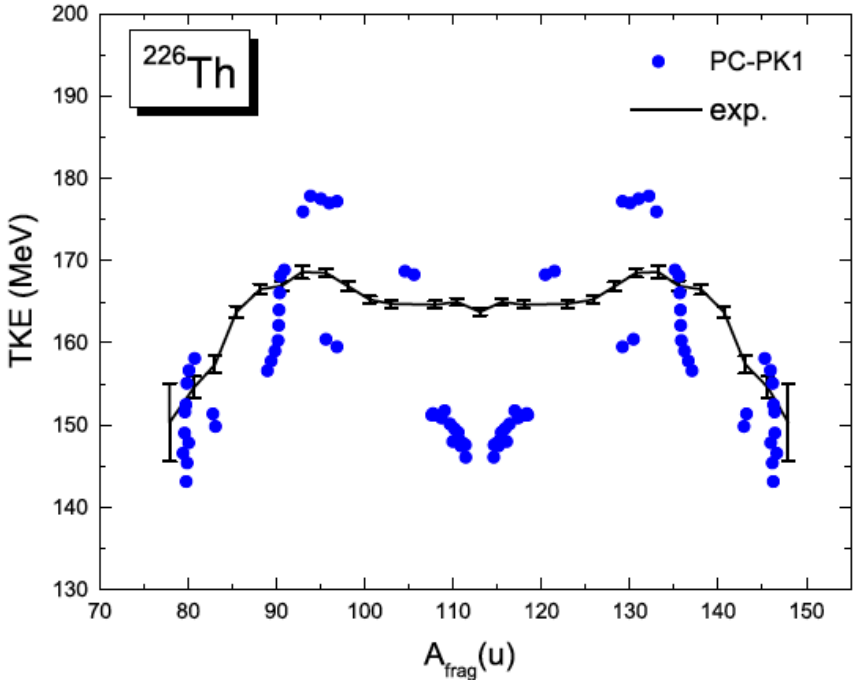

Figure 2. *The calculated total kinetic energy of the nascent fission fragments for ^{226}Th as a function of fragment mass, in comparison to the data [26].*

The total kinetic energy (TKE) for a particular pair of fragments can be evaluated from

$$E_{TKE} = \frac{e^2 Z_H Z_L}{d_{ch}} \tag{6}$$

where e is the proton charge, Z_H (Z_L) the charge of the heavy (light) fragment, and d_{ch} the distance between fragment centers of charge at scission.

Figure 2 displays the calculated total kinetic energies of the nascent fission fragments for ^{226}Th as a function of fragment mass. For comparison, the data obtained in photoinduced fission measurement [26] are also included in the figure. One notices that the theoretical results qualitatively reproduce the trend of the data, in particular the maxima for A_{frag}~132 and A_{frag}~94. On a quantitative level the calculation exhibits more structure when compared to experiment. This may be due to the fact that the experimental values correspond to an excitation energy of the fissioning nucleus of the order of 11 MeV, whereas formula (6) is valid only for low–energy fission. As it is well known, the kinetic energy distribution is generally smoothed out as the fission energy increases. In particular, the kinetic energy in the symmetric mass region increases [31], which explains why experimental TKEs display only a very shallow minimum for A_{frag}=A/2. We note that the present theoretical results are consistent with those obtained using the Gogny D1S effective interaction in Ref. [29].

Figures 3 and 4 display the scission lines in the β_2-β_3 plane and the TKEs of nascent fission fragments of ^{226}Th, respectively, for three different values of the pairing strength. The pattern of the scission line does not change significantly, except at the bending points and, overall, a smoother contour is obtained for stronger pairing. We also note that the scission points on the static fission path for three values of the pairing strength are very close to each other, at (β_2,β_3) ~ (3.3,2.0). This result differs from that in ^{240}Pu calculated using the HFB method with the Skyrme functional SkM* [32], where the quadrupole deformation β_2 at the scission point changes by as much as ~0.65 when the original pairing strength is varied from 90% to 110%. Since the TKEs in the present study are fully determined by the scission configurations, varying the pairing strength does not lead to marked differences in the TKE distribution.

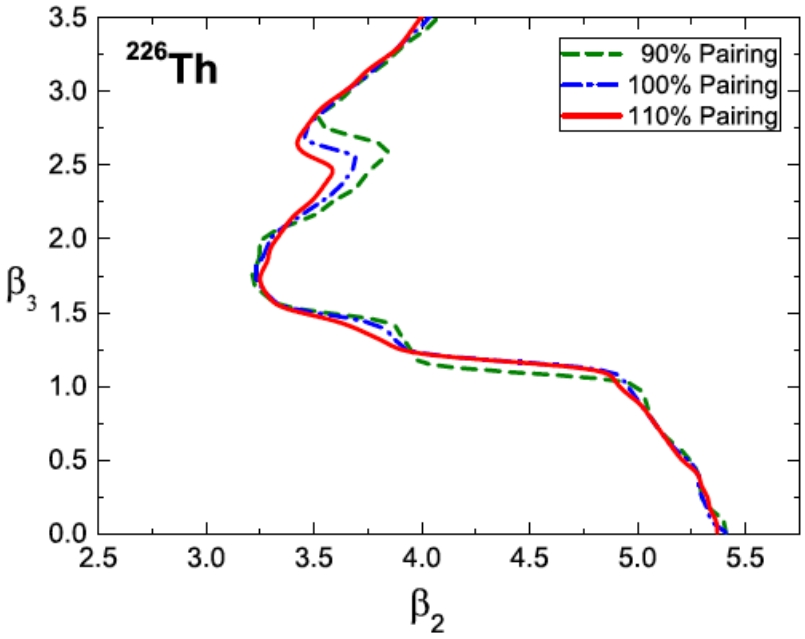

Figure 3. *The scission lines for ^{226}Th in the β_2–β_3 plane, obtained in calculations with three different values of the pairing strength.*

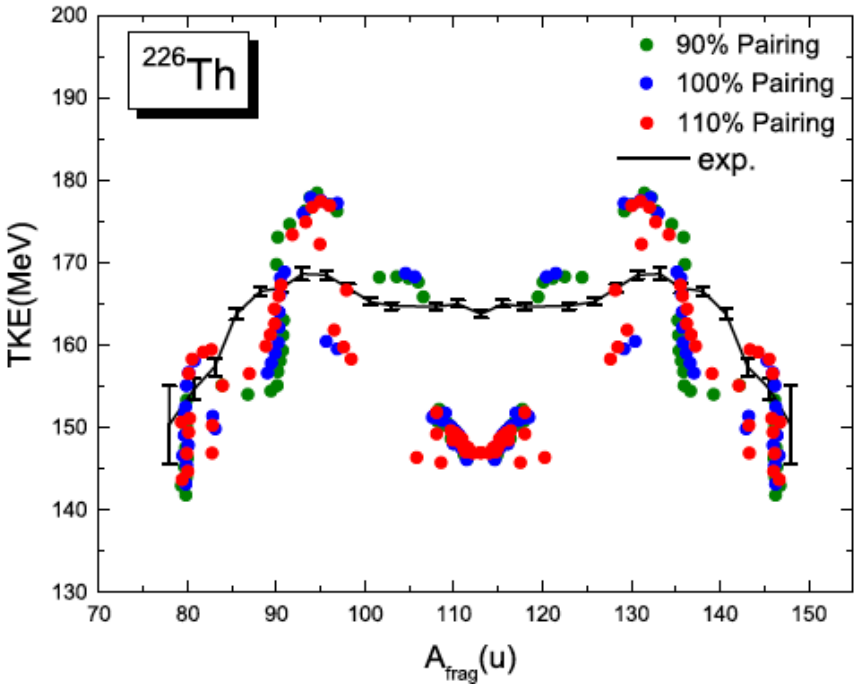

Figure 4. *Comparison between experimental and calculated total kinetic energy of nascent fission fragments for ^{226}Th, as a function of fragment mass and pairing strength.*

In Fig. 5 we compare the charge yields, obtained with three different pairing strengths, to the data for photoinduced fission of ^{226}Th. Following the procedure of Ref. [24], the initial state is prepared by boosting the collective ground state in the direction of increasing axial quadrupole deformation. The amplitude of the boost is determined so that the average energy of the initial state is ~1 MeV above the corresponding asymmetric fission barrier B^{asy}_{II} of the collective potential energy surface. The calculation reproduces the trend of the data, except that obviously the model cannot describe the odd-even staggering of the experimental charge yields. For weak pairing correlations, that is, at 90% of the

original pairing strength, the yields are dominated by asymmetric fission with peaks at Z = 35 and Z = 55. A broad peak corresponding to symmetric fission is also predicted but is too low compared to data. This is because the asymmetric fission barrier B^{asy}_{II} is ~6 MeV lower than the symmetric one B^{sym}_{II}. The asymmetric peaks are reduced and the symmetric peak enhanced as pairing correlations increase, and we find that the data are best reproduced by a pairing strength between 100% and 110% of the original parameters. This can be attributed to a reduction of the ridge between asymmetric and symmetric fission valleys when increasing the pairing strength. Another important effect is that the wavelength becomes longer because of smaller collective masses for stronger pairing, and this enhances the collective current in the symmetric fission valley beyond $\beta_2 > 2.5$.

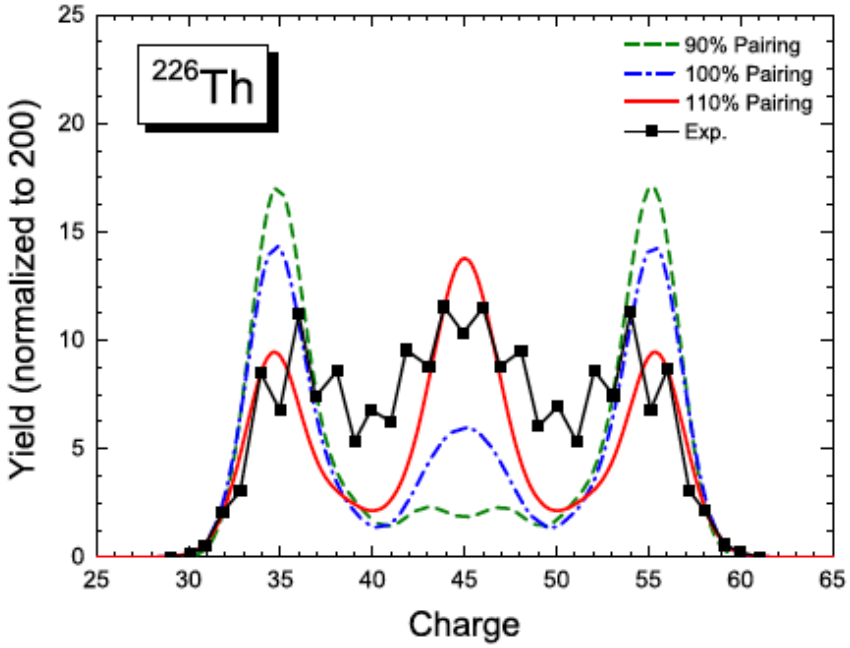

Figure 5. *Preneutron emission charge yields for photoinduced fission of ^{226}Th. The results of calculations for three different values of the pairing strength are compared to the data [26].*

CONCLUSIONS

The dynamics of induced fission of ^{226}Th has been analyzed in a theoretical framework based on covariant energy density functionals and the corresponding collective Hamiltonian, making use of a recently developed numerical implementation of the time-dependent generator coordinate method plus Gaussian overlap approximation [23]. The potential energy surface, scission line, and total kinetic energies have been calculated using the multidimensionally constrained relativistic mean–field model based on the energy density functional PC–PK1, and with pairing correlations taken into account in the BCS approximation. The fission process is described in a two-dimensional axially symmetric collective space (β_2, β_3).We note that the overall topography of the PES, the total kinetic energies for a particular pair of fragments, and the general pattern of the scission line are consistent with previous studies based on the Gogny effective interaction [29,30].

The TDGCM+GOA calculation reproduces the main characteristics of the fission charge and mass distributions, thus confirming the main conclusion of the analysis presented in Ref. [24]. In this study we have analyzed the influence of ground–state pairing on the preneutron emission charge yields. The increase of static pairing correlations reduces the asymmetric peaks and enhances the symmetric peak in charge yields distribution. Therefore a very interesting topic for future studies is dynamic pairing correlation in induced fission, possibly through the inclusion of pairing degrees of freedom in the space of TDGCM+GOA collective coordinates.

Acknowledgments

This research was conducted within the Call “Fellowship for Postodoctoral research” implemented by the University of Thessaly and funded by the Stavros Niarchos Foundation.

References

[1] Jie Zhao et al., Phys. Rev. C 99 014618 (2019), doi: 10.1103/PhysRevC.99.014618
[2] N. Schunck and L. M. Robledo, Rep. Prog. Phys. 79, 116301 (2016), doi: 10.1088/0034-4885/79/11/116301
[3] Hans J. Krappe and K. Pomorski, Theory of Nuclear Fission (Springer-Verlag, Berlin, 2012).
[4] G. Scamps, C. Simenel, and D. Lacroix, Phys. Rev. C 92, 011602(R) (2015), doi: 10.1103/PhysRevC.92.011602
[5] C. Simenel and A.S. Umar, Phys. Rev. C 89, 031601(R) (2014), doi: 10.1103/PhysRevC.89.031601
[6] P. Goddard, P. Stevenson, and A. Rios, Phys. Rev. C 92, 054610 (2015), 10.1103/PhysRevC.92.054610
[7] B. Avez, C. Simenel, and P. Chomaz, Phys. Rev. C 78, 044318 (2008), 10.1103/PhysRevC.78.044318
[8] A. Bulgac et al., Phys. Rev. Lett. 116, 122504 (2016), doi: 10.1103/PhysRevLett.116.122504
[9] P. Goddard, P. Stevenson, and A. Rios, Phys. Rev. C 93, 014620 (2016), doi: 10.1103/PhysRevC.93.014620
[10] Y. Tanimura, D. Lacroix, and S. Ayik, Phys. Rev. Lett. 118, 152501 (2017), doi: 10.1103/PhysRevLett.118.152501
[11] T. Nakatsukasa et al., Rev. Mod. Phys. 88, 045004 (2016), doi: 10.1103/RevModPhys.88.045004
[12] S. A. Giuliani, L.M. Robledo, and R. Rodriguez-Guzman, Phys. Rev. C 90, 054311 (2014), doi: 10.1103/PhysRevC.90.054311
[13] C. R. Chinn et al., Phys. Rev. C 45, 1700 (1992), doi: 10.1103/PhysRevC.45.1700
[14] A. Staszczak, A. Baran, and W. Nazarewicz, Phys. Rev. C 87, 024320 (2013), doi: 10.1103/PhysRevC87.024320
[15] M. Warda and J. L. Egido, Phys. Rev. C 86, 014322 (2012), doi: 10.1103/PhysRevC.86.014322
[16] J. W. Negele, Rev. Mod. Phys. 54, 913 (1982), doi: 10.1103/RevModPhys.54.913
[17] J. Sadhukhan et al., Phys. Rev. C 88, 064314 (2013), doi: 10.1103/ PhysRevC.88.064314
[18] J. Sadhukhan et al., Phys. Rev. C 90, 061304 (2014). doi: 10.1103/ PhysRevC.90.061304
[19] R. Smolanczuk, J. Skalski, and A. Sobiczewski, Phys. Rev. C 52, 1871 (1995), doi: doi: 10.1103/ PhysRevC.52.1871
[20] J. F. Berger, M. Girod, and D. Gogny, Comp. Phys. Comm. 63, 365 (1991), doi: 10.1016/0010-4655(91)90263-K
[21] H. Goutte, J. F. Berger, P. Casoli, and D. Gogny, Phys. Rev. C 71, 024316 (2005), doi: 10.1103/PhysRevC.71.024316
[22] W. Younes and D. Gogny, Lawrence Livermore National Laboratory Report No. LLNL-TR-586678, 2012 (unpublished).
[23] D. Regnier et al., Comp. Phys. Comm. 200, 350 (2016), doi: 10.1016/j.cpc.2015.11.013
[24] D. Regnier et al., Phys. Rev. C 93, 054611 (2016), doi: 10.1103/PhysRevC.93.054611
[25] A. Zdeb, A. Dobrowolski, and M. Warda, Phys. Rev. C 95, 054608 (2017), doi: 10.1103/PhysRevC.95.054608
[26] K.-H. Schmidt, et al., Nucl. Phys. A 665, 221 (2000), doi: 10.1016/S0375-9474(99)00384-X
[27] P. W. Zhao et al., Phys. Rev. C 82, 054319 (2010), doi: 10.1103/PhysRevC.82.054319
[28] M. Bender et al., Eur. Phys. J. A 8, 59 (2000), doi: 10.1007/s10050-000-4504-z
[29] N. Dubray, H. Goutte, and J.-P. Delaroche, Phys. Rev. C 77, 014310 (2008), doi: 10.1103/PhysRevC.77.014310
[30] W. Younes and D. Gogny, Phys. Rev. C 80, 054313 (2009), doi: 10.1103/PhysRevC.054313
[31] S. Pommé et al., Nucl. Phys. A 572, 237 (1994), doi: 10.1016/0375-9474(94)90174-0
[32] N. Schunck, D. Duke, H. Carr, and A. Knoll, Phys. Rev. C 90, 054305 (2014), doi: 10.1103/PhysRevC.90.054305